JACS
JOURNAL OF THE AMERICAN CHEMICAL SOCIETY
Article
Cite This: J. Am. Chem. Soc. 2018, 140, 4144−4149
pubs.acs.org/JACS

Supported Au Nanoparticles with *N*-Heterocyclic Carbene Ligands as Active and Stable Heterogeneous Catalysts for Lactonization

Rong Ye,[†,‡,⊥,¶,#] Aleksandr V. Zhukhovitskiy,[†,#] Roman V. Kazantsev,[†,§] Sirine C. Fakra,[∥] Brent B. Wickemeyer,[†] F. Dean Toste,*[,†,‡] and Gabor A. Somorjai*[,†,‡,⊥]

[†]Department of Chemistry, [⊥]Kavli Energy NanoScience Institute, University of California, Berkeley, Berkeley, California 94720, United States

[‡]Chemical Science Division, [§]Joint Center for Artificial Photosynthesis, [∥]Advanced Light Source, Lawrence Berkeley National Laboratory, 1 Cyclotron Road, Berkeley, California 94720, United States

Supporting Information

ABSTRACT: Attachment of *N*-heterocyclic carbenes (NHCs) on the surface of metal nanoparticle (NP) catalysts permits fine-tuning of catalytic activity and product selectivity. Yet, NHC-coated Au NPs have been seldom used in catalysis beyond hydrogenation chemistry. One challenge in this field has been to develop a platform that permits arbitrary ligand modification without having to compromise NP stability toward aggregation or leaching. Herein, we exploit the strategy of supported dendrimer-encapsulated metal clusters (DEMCs) to achieve aggregation-stable yet active heterogeneous Au NP catalysts with NHC ligands. Dendrimers function as aggregation-inhibitors during the NP synthesis, and NHCs, well-known for their strong attachment to the gold surface, provide a handle to modify the stereochemistry, stereoelectronics, and chemical functionality of the NP surface. Indeed, compared to "ligandless" Au NPs which are virtually inactive below 80 °C, the NHC-ligated Au NP catalysts enable a model lactonization reaction to proceed at 20 °C on the same time scale (hours). Based on Eyring analysis, proto-deauration is the turnover-limiting step accelerated by the NHC ligands. Furthermore, the use of chiral NHCs led to asymmetric induction (up to 16% enantiomeric excess) in the lactonization transformations, which demonstrates the potential of supported DEMCs with ancillary ligands in enantioselective catalysis.

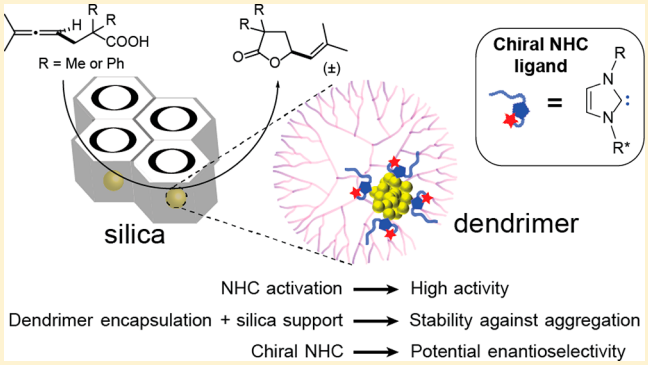

INTRODUCTION

Supported dendrimer-encapsulated metal clusters (DEMCs) are highly active and easily recyclable catalysts, which have enabled new supported catalysis methodology.[1] However, despite its broad utility, this catalyst platform presently lacks a modular handle to tune reaction outcomes. Yet, rapid optimization of catalyst performance metrics such as reactivity, enantio-, diastereo-, regio-, and chemo-selectivity would greatly advance the sophistication and scope of transformations catalyzed by DEMCs. Ancillary ligands, commonly utilized in transition metal catalysis to tune catalyst selectivity, were a logical choice of the desired modular handles to be added to DEMCs. Among a broad array of ligands, persistent carbenes (PCs, also known as stable carbenes;[2] e.g., *N*-heterocyclic carbenes, or NHCs[3]) offer numerous advantages: (1) strong binding to a broad array of elements,[4] which in many cases has enabled the stabilization and isolation of highly reactive chemical species,[5] (2) improved oxidative stability compared to ligands like phosphines and thiolates,[6] and (3) synthetic accessibility and modularity.[5,7] In addition, the judicious choice of NHCs as ligands on metal nanoparticle (NP) surfaces has been shown as a versatile strategy to enable selective heterogeneous catalysis,[8] with pioneering work by Glorius[3a,8b−f] and Chaudret.[8g−j] So far, most examples of NHC-ligated NP catalysis focused on Pd, Pt, and Ru, and with the exceptions of three reports (enantioselective ketone arylation[8b] and aldehyde allylation;[8c] Buchwald−Hartwig amination[8f]) nearly all of the examples describe hydrogenation catalysis.[8e,g−j] Despite the broad scope of known gold-catalyzed transformations[9] and the growing body of work on NHC-Au surface chemistry,[5,6b,10] catalysis by NHC-ligated Au NPs has been scarcely explored, and to our knowledge, only been applied to hydrogenation chemistry or electrochemical CO_2 reduction.[8k,l,11] A main challenge has been to systematically vary the ligand structure without perturbing Au NP stability to Au complex leaching and/or NP aggregation. Work in our laboratories on supported dendrimer encapsulated Au NPs[1d−f] provided a platform for overcoming this challenge.

Herein, we combine the strategies of supported DEMCs and NHC-ligated nanoparticles for the facile synthesis of catalytically active yet stable heterogeneous gold catalysts for a model

Received: January 26, 2018
Published: March 5, 2018

© 2018 American Chemical Society

DOI: 10.1021/jacs.8b01017
J. Am. Chem. Soc. 2018, 140, 4144−4149

lactonization reaction with the possibility of ligand-derived enantioinduction (Figure 1). To the best of our knowledge, this

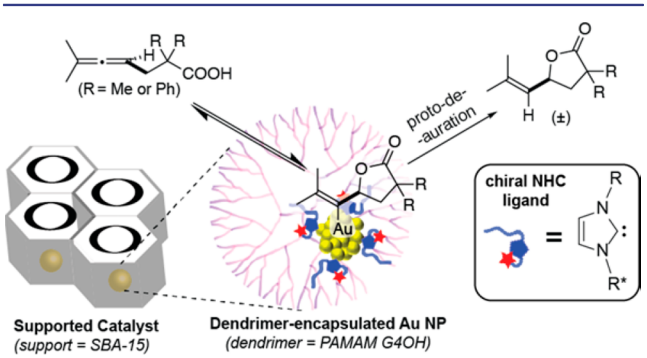

Figure 1. An illustration of the supported dendrimer-encapsulated NHC-ligated Au NPs and the catalytic lactonization reaction they catalyze. A putative mechanism based on analogous transformations (*vide infra*) is shown. Fourth-generation hydroxyl-terminated polyamidoamine dendrimer (PAMAM G4OH, or G4OH for short) is utilized in this work.

is the first report of DEMCs with NHC ligands, as well as of NHC-ligated Au NP catalysis extended beyond hydrogenation or CO_2 reduction: namely, lactonization of allene-carboxylic acids. This model lactonization reaction was chosen because gold complexes, homogeneous[12] or loaded in molecular form onto silica,[13] have been previously shown to successfully catalyze this transformation in enantioselective fashion. Given the often ambiguous oxidation state, as well as distinct coordination environment and ligand presentation at a Au NP surface compared to molecular Au(I) species, translation of homogeneous reactivity to Au NPs is a known challenge. However, this challenge is also an opportunity to utilize the distinctly nanoparticle-derived handles (e.g., under-coordinated surface sites) on reactivity and selectivity. The synthesis, characterization, and proof-of-principle reaction studies of these catalysts will be discussed in detail.

EXPERIMENTAL SECTION

Synthesis of Cat-0. The synthesis of NHC-free Au NP catalyst, stabilized with the fourth generation hydroxyl-terminated polyamidoamine dendrimer (G4OH) supported in SBA-15, i.e., Au_{40}/G4OH/SBA-15 (**Cat-0**, see Table 1 for the meanings of sample codes used in this publication) was reported elsewhere.[1d,f,14] Briefly, a stock solution of G4OH in water containing 1.5 μmol of G4OH was diluted to 52 mL in a 100 mL round-bottomed flask, and purged with argon for half an hour. 0.01 M $HAuCl_4$ (6 mL) was then added into the flask dropwise with vigorous stirring. Immediately afterward, a 20-fold excess of a freshly prepared mixture of 0.5 M $NaBH_4$ and 0.15 M NaOH (stored at 0 °C before use) was injected dropwise into the flask with vigorous stirring. The yellow solution turned dark immediately, and was then stirred for 3 h, after which it was purified by dialysis against deionized water in cellulose dialysis tubes. Next, SBA-15 was added to the colloidal solution of NPs and the mixture was sonicated for 3 h at room temperature. The NP supported SBA-15 was separated from the solution by centrifuge at 4,200 rpm for 6 min. After centrifugation, the solution was clear. The solution was then decanted, and the catalyst was dried at 80 °C overnight. The resultant catalyst (**Cat-0**) was a purple powdery solid.

Synthesis of Cat-1. In a 4 mL glass vial, 0.01 mmol (5.19 mg) of the **1** was dissolved in 1.0 mL of chloroform (Solution 1), and 986 mg of a 7.24 wt % solution of G4OH in methanol containing 5 μmol of G4OH was diluted to 1.0 mL with methanol (Solution 2). Solution 1 and Solution 2 were mixed with stirring for 1.5 h in the dark. 1 mmol of *tert*-butylamine-borane complex (8.70 mg) was added as a solid in one portion with vigorous stirring. The colorless solution gradually turned purple. After 1 h, the resultant solution of nanoparticles (**Au/G4OH-NP-1**) was sonicated with 150 mg of mesoporous silica SBA-15 for 2 h, washed with 40 mL of chloroform three times (the liquid was decanted after centrifugation at 4,200 rpm for 6 min), and dried at 80 °C overnight to obtain the final catalyst (**Cat-1**) as a pink-colored powdery solid.

Detailed procedures of the synthesis and characterization of the catalyst precursors, reactants, and other nanoparticles containing various portions of components are included in the SI.

RESULTS AND DISCUSSION

Catalyst Design and Synthetic Strategy. We sought to install an NHC ligand due to its strong surface binding and versatility as an ancillary ligand.[3a,5] Looking ahead to exploring enantioselective lactonization, we desired a stereogenic center in one of the *N*-substituents; specifically, we selected the ligand in complex **1** (Figure 2) because it was readily available, derived from an L-amino acid (which suggested a modular approach to chiral ligand diversification), and previously demonstrated to induce high enantioselectivity in conjugate additions catalyzed by Cu(II).[15] Furthermore, the presence of a hydroxyl group in the ligand structure could potentially strengthen interactions of the NHC-ligated AuNP with SBA-15, improving the catalyst stability, and it could also facilitate proto-deauration, a step that had been previously postulated to be turnover-limiting for the transformation at hand,[13] and demonstrated to be turnover-limiting in intramolecular allene-alcohol etherification.[16] The synthesis and characterization of **Cat-1** and **Cat-0** are summarized and compared in Figure 2. As described in the previous section, whereas $HAuCl_4$ was reduced in water to obtain **Au/G4OH-NP-0**, the NHC precursor **1** was not readily soluble in water. Thus, a methanol/chloroform 1:1 v/v mixture was used as the solvent. Following the versatile "Stucky method"[17] for nanoparticle synthesis, the *tert*-butylamine-borane complex was chosen as the reducing agent due to its

Table 1. Sample Codes and the Corresponding Compositions of the Gold Samples

Codes[a]	Composition
Cat-0	Au_{40}/G4OH/SBA-15
Au/G4OH-NP-0	Au_{40}/G4OH (aqueous solution) before loading onto SBA-15
1	NHC-Au(I)-Cl complex as the precursor for Au NPs, see Figure 1 for the chemical structure
Au/G4OH-NP-1	Au NPs (methanol/chloroform solution) prepared from the reduction of **1** in the presence of G4OH
Cat-1	**Au/G4OH-NP-1** loaded onto SBA-15
AuNP-1	Au NPs (methanol/chloroform solution) prepared from the reduction of **1** in the absence of G4OH
AuNP-1/SBA-15	**AuNP-1** loaded onto SBA-15 as a solid
IS-1	the precursor imidazolium salt of **1**

[a]The codes containing **2**, **3**, ..., **11** are used in the same way as the codes containing **1**, which is illustrated in Figure 4.

DOI: 10.1021/jacs.8b01017
J. Am. Chem. Soc. 2018, 140, 4144−4149

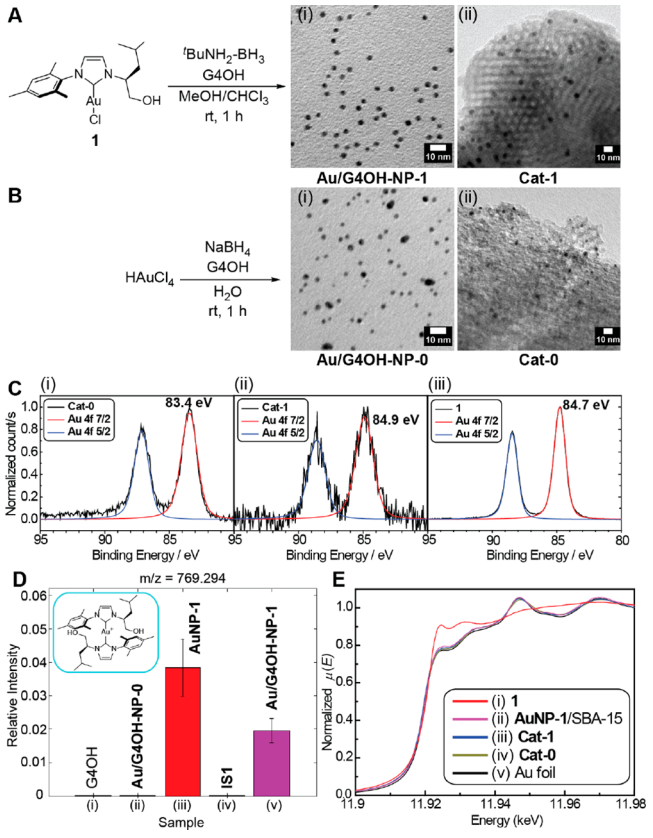

Figure 2. (A and B) Preparation and TEM images of nanoparticles in **Cat-1** (A) and **Cat-0** (B) before (*i*) and after (*ii*) loading into SBA-15, respectively. (C) Normalized Au 4f XPS spectra of **Cat-0** (*i*), **Cat-1** (*ii*), and **1** (*iii*). (D) Relative intensity of the mass-to-charge ratio of 769.294 from ToF-SIMS spectra of G4OH (*i*), **Au/G4OH-NP-0** (*ii*), **AuNP-1** (*iii*), **IS1**, i.e., the precursor imidazolium salt of **1** (*iv*), and **Au/G4OH-NP-1** (*v*). Inset: the proposed structure of the ion whose mass-to-charge ratio matches 769.294. (E) Au L3-edge XANES spectra of **1** (*i*), **AuNP-1**/SBA-15 (*ii*), (c) **Cat-1** (*iii*), **Cat-0** (*iv*), and a gold foil (*v*).

previously demonstrated success in forming NHC-ligated gold nanoparticles.[10e,18] The average sizes of both as-synthesized NPs were comparable (ca. 3 nm in diameter). However, NPs in **Cat-1** were still growing during the loading process due to continued reduction of **1**, ultimately reaching a diameter of ∼4.7 nm; meanwhile, the NPs in **Cat-0** remained the same average size as before loading (Figure 2A,B). The observed size NP difference between **Cat-0** and **Cat-1** proved inconsequential with regard to their activity, given the results for other catalysts described herein (*vide infra;* Tables S1 and S2).

The use of dendrimer enhances the stability of the NPs to aggregation on the time scale of their synthesis, and inhibits their fusion at longer time scales. The morphology evolution of **Au/G4OH-NP-1** and **AuNP-1** under otherwise identical synthetic conditions was monitored by TEM (Figure S1). **Au/G4OH-NP-1** existed as isolated NPs at the 8th hours after the reduction, but at the same time a large portion of NPs of **AuNP-1** aggregated to particles >10 nm in diameter. At the 32nd hour after the reduction step, individual NPs of ca. 5 nm in size were still observed in **Au/G4OH-NP-1**: some aggregated, but, retained separate boundaries; in the case of **AuNP-1**, large aggregates of particles fused together by this point. In addition, reduction of other NHC-Au(I) complexes led to NPs of broad size distributions even at early stages of complex reduction, but addition of the dendrimer resolved this issue. Thus, the dendrimers functioned as a stabilizer of the NPs.

Besides the reduction of structurally well-defined NHC-Au(I) complexes, e.g. **Au-1**, to prepare **Cat-1**, another method was attempted to attach the NHC to the Au surface:[6a,10d,h] namely, via CO_2 adducts of *N*-heterocyclic carbenes (NHC-CO_2). However, the surface modification method led to the aggregation of Au particles under the conditions we tested (Figure S2). Thus, this method was not used further in this work.

Au Oxidation State Analysis. X-ray photoelectron spectroscopy (XPS) analysis shed light on the oxidation state differences at the Au NP surfaces (Figure 2C). The Au $4f_{7/2}$ binding energy of **Cat-0** was 83.4 eV, consistent with nanoparticular Au(0): Kruse and Chenakin[19] previously observed that the charge-corrected Au $4f_{7/2}$ binding energy in Au NP/TiO_2 catalysts was 0.15−0.45 eV lower than that in the pure bulk Au. In contrast, the Au $4f_{7/2}$ binding energy observed for **Cat-1** was 84.9 eV, similar to that of the Au(I) complex **1** (84.7 eV). This difference of ∼1.5 eV between **Cat-1** and **Cat-0** reflected the prevalence of Au(I) species at the surface of the former and Au^0 at the surface of the latter. To understand how far beyond the very surface the oxidation state differences persisted, we turned to X-ray absorption near edge structure (XANES), a bulk analysis technique. XANES of complex **1** was analogous to that of another NHC-Au(I) chloride reported by Silbestri and colleagues,[20] whereas the spectra of both **Cat-1** and **Cat-0** where quite different, and nearly identical to that of a gold foil (Figure 2E). Linear combination analyses using the spectra of **Au-1** and the Au foil as the basis set indicated that over 95% of Au atoms in **Cat-1** and **Cat-0** are in the Au(0) phase. In addition, *in situ* XANES spectra of **Cat-1** under the catalytic reaction conditions, i.e., in the presence of the reactant and solvent (*vide infra*), remain the same as the *ex situ* spectra (Figure S5). Thus, the particles do not undergo oxidative degradation (e.g., to Au(I) complexes) on the time scale of the reaction. Based on XPS and XANES, we can therefore conclude that the Au NPs of **Cat-1** are coated with a ∼ monolayer of Au(I) species, presumably NHC-Au(I) complexes. Such monolayers of NHC-oxidized metal species at metal NP and bulk metal surfaces have a number of recent precedents.[8i,21]

Time-of-flight secondary ion mass spectrometry (ToF-SIMS) provided additional evidence for the presence of NHC-Au complexes at the surfaces of **AuNP-1** and **Au/G4OH-NP-1** (**Cat-1** was not directly analyzed because ToF-SIMS typically cannot probe below the very surface of the given material). Namely, both samples exhibited a mass-to-charge ratio (*m*/*z*) of 769.294 (Figure 2D) and associated isotope pattern (Figure S4), attributable to the corresponding $(NHC)_2Au^+$ ion (theoretical *m*/*z* = 769.375, Figure 2D inset). Furthermore, when the as-synthesized sample was purified via dialysis against methanol, dried and redispersed in CD_3OD, the ^1H NMR spectrum revealed the presence of two sets of broadened NHC-derived aromatic resonances; meanwhile, other reaction components (e.g., **1** and $^tBuNH_2{\cdot}BH_3$ byproducts) were absent (Figure S35). The presence of two sets instead of one suggests the presence of multiple NHC-Au species at the Au NP surface. Together, TEM, XPS, XANES, ToF-SIMS, and ^1H NMR analyses allow us to infer that **Cat-1** is composed of ∼4.7 nm-diameter nanoparticles whose core of Au^0 is coated with NHC-Au(I) complexes such as $(NHC)Au^+$ and $(NHC)_2Au^+$. Whereas the latter coordinatively saturated Au(I) species is unlikely to be active in our transformation, the under-

DOI: 10.1021/jacs.8b01017
J. Am. Chem. Soc. 2018, 140, 4144−4149

coordinated surface gold atoms, including (NHC)Au^+ were considered plausible catalytically active sites.

Catalytic Studies. Intramolecular lactonizations of allenes (Figure 1) were chosen as model reactions to evaluate the effect of Au NP surface composition on its performance under a diverse set of conditions. Note that while molecular Au(I) complexes dispersed in mesoporous silica were previously found to be active catalysts for this reaction, formation of Au NPs under reaction conditions actually led to reduced activity over time.[13] Indeed, Au NP-catalyzed lactonization of allenes remains a challenge, and we address this limitation herein. **Cat-1** readily catalyzes the lactonization of reactant **A** at room temperature in predeuterated dichloromethane (CD_2Cl_2), benzene (C_6D_6), and chloroform ($CDCl_3$) (Table 2), and

Table 2. Reaction Condition Screening and Comparison of Cat-1 and Cat-0

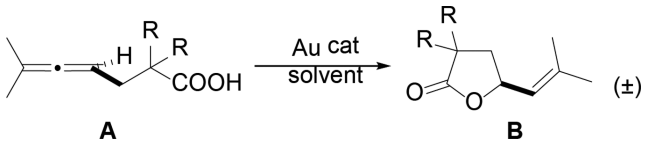

A **B**

catalyst	Au mol %	solvent	temperature (°C)	time (h)	yield[a] (%)
Cat-1	2.2	CD_2Cl_2	20	2	29
Cat-1	2.2	C_6D_6	20	2	21
Cat-1	2.2	$CDCl_3$	20	2	12
Cat-1	2.2	CD_2Cl_2	20	22	100
Cat-0	3.6	CD_2Cl_2	20	22	<1
Cat-0	3.6	Tol-d_8	80	2	7
Cat-0	3.6	Tol-d_8	100	22	100

[a]The yield was determined by ^{1}H NMR using 1,1,2,2-tetrachloroethane as an internal standard.

CD_2Cl_2 provided the highest reaction rate. Notably, though **Cat-1** can achieve full conversion of **A** within 22 h at room temperature (20 °C), **Cat-0** shows no reactivity under the same conditions. Even at 80 °C (in toluene-d_8), **Cat-0** shows little activity and requires 100 °C to reach full conversion of **A** within 22 h. Thus, the presence of NHC complexes on the surface of **Cat-1** is critical to engender the catalyst with high activity even at room temperature.

The reaction stops immediately upon the filtration of **Cat-1**, which confirms that the catalysis is truly heterogeneous. The heterogeneity of the catalyst was also confirmed by the inductively coupled plasma optical emission spectroscopy (ICP-OES) tests of the filtrate of the reaction mixture after reaction, where the Au concentration was below the 0.1 ppm detection limit of the instrument. The analysis procedure is included in the SI. TEM images of **Cat-1** after the catalytic reaction show no apparent change of morphologies compared to the as-synthesized **Cat-1**. It can be reused for at least four additional runs (Figure S6) without a loss of activity, which also confirmed the stability of the catalyst.

The reaction kinetics of **A** and its analogue **A′** were investigated to better understand the effect of the catalyst on reaction mechanism (Figure 3A). Lactonization of **A** follows overall first-order kinetics as indicated from the linear ln[**A**]−time plot (Figure 3B). Eyring analysis (Figure 3C) covering a 63 °C temperature range (248 to 311 K) revealed the following kinetic parameters for **A** and **A′**, respectively: $\Delta H^{\ddagger}$ of 6.4 ± 0.4 and 7.9 ± 1.0 kcal·mol^{-1}, $\Delta S^{\ddagger}$ of −57 ± 2 and −52 ± 3 cal·mol^{-1}·K^{-1}, respectively. The small $\Delta H^{\ddagger}$ and large negative $\Delta S^{\ddagger}$

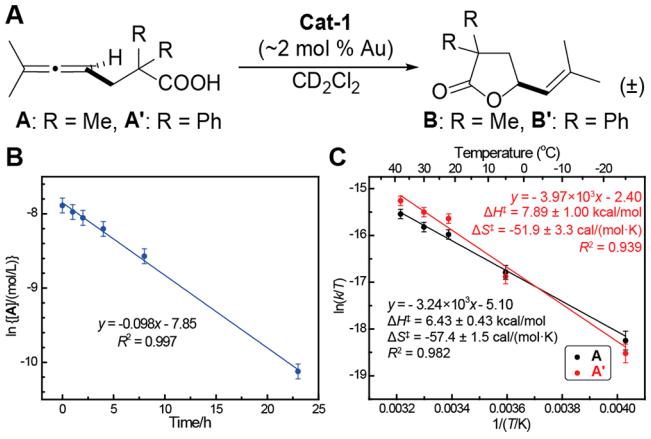

Figure 3. Kinetics studies of the lactonization reaction catalyzed by **Cat-1**. (A) Reaction scheme. (B) Plot of ln[**A**] vs time showing first-order kinetics. The reaction was performed in an NMR tube with constant shaking at room temperature. (C) Eyring plot of **A** and **A′** along with the corresponding $\Delta H^{\ddagger}$ and $\Delta S^{\ddagger}$. Each reaction was run for 2 h.

values are consistent with proto-deauration as the turnover-limiting step, a common scenario in Au(I) catalysis, which has been previously postulated in Au(I)-catalyzed allene lactonizations.[13] Notably, Roth and Blum[22] observed that the presence of the NHC ligand nearly doubled the rate of proto-deauration compared to the analogous triphenylphosphine complex. In line with this experimental study, theoritical studies by Belanzoni and colleagues[23] showed that electron-donating ligands reduce the electrostatic component of the Au−C bond undergoing proto-deauration, which in turn reduces the activation barrier for this process. Given that NHCs are some of the most strongly electron-donating ancillary ligands,[24] the observed high activity of **Cat-1** compared to **Cat-0** is reasonable.

Inspired by the initial success of **Cat-1**, we sought to expand the catalyst scope (Figure 4). The catalyst analogues **Cat-2**−**Cat-11** were prepared similarly to **Cat-1**. The details of the synthesis and characterization of the NHC-Au(I) complexes (catalyst precursors shown in Figure 4) and the catalysts are included in the SI (TEM images see Figure S7 and statistics analyses in Table S2). Generally, Au NPs in **Cat-2**−**Cat-8** have relatively uniform size distributions, ranging from 2 to 7 nm in diameter. **Cat-9**−**Cat-11**, however, contain Au NPs larger than 10 nm. XPS analysis of these new catalysts indicated that the surface Au 4f 7/2 binding energy varied considerably with the NHC: **Cat-5** (85.7 eV) > **Cat-1** (84.7 eV) > **Cat-2**−**Cat-4**, **Cat-10** (83.8−84.3 eV) > **Cat-6**−**Cat-8** (83.5−83.7 eV) > **Cat-0** (83.4), **Cat-11** (82.9 eV) (Figure S8). This variation indicated that the distribution of Au oxidation states at the NP surface could be tuned using different NHCs.

As in the case of **Cat-1**, for most new catalysts, **A′** underwent lactonization faster than **A** at 20 °C. **Cat-1**−**Cat-8** all catalyze full conversion of **A′** in 22 h, although **Cat-8** cannot accomplish the same for **A**. The turnover frequencies (TOF, normalized to the total amount of Au) based on the 2 h reactions of **A** under the same conditions reflect the catalytic activity of each catalyst. Several valuable conclusions were derived from these results. First, the presence of one mesityl *N*-substituent on the NHC ligand led to an elevated TOF per Au (cf. **Cat-1** vs **Cat-6**, and **Cat-4** vs **Cat-7**). This observation is consistent with the activating influence of an aryl-surface interaction recently

DOI: 10.1021/jacs.8b01017
J. Am. Chem. Soc. 2018, 140, 4144−4149

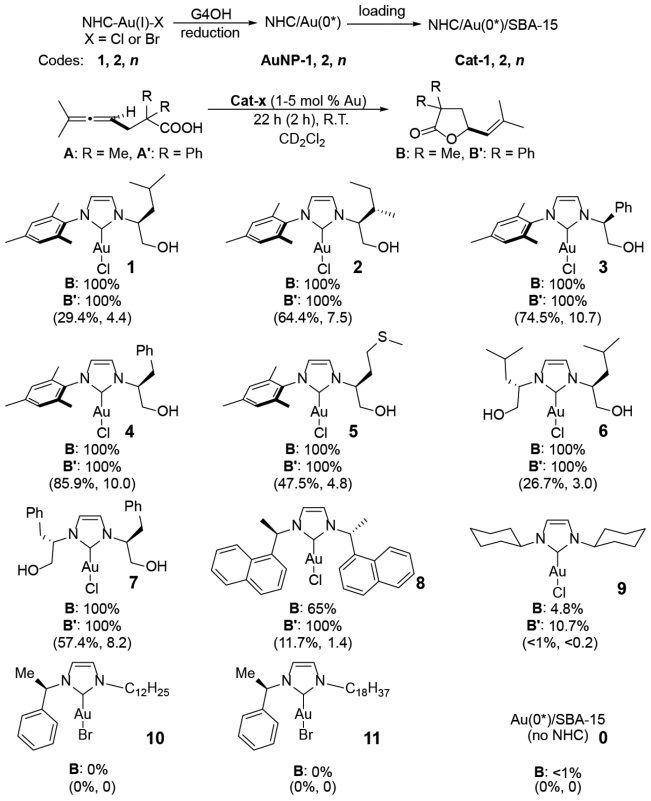

Figure 4. Schematics of the synthesis of the final supported catalysts **Cat-*n*** with the NHC structure corresponding to the sample code. The yields of the 22 h reactions of **A** and **A′** (and 2 h reactions of **A** in the parentheses and the corresponding TOF in the unit of h^{-1} based on total Au atoms) catalyzed by **Cat-*n*** are given below each structure. Even though the catalysts are prepared in the same scale and conditions, the molar percentage of Au in the catalysts are different. As a fixed weight (10 mg) of each catalyst is used, the mol % of Au of each catalyst is different.

demonstrated by Glorius and co-workers.[8f] The increase in activity in the order **Cat-1**, **Cat-2**, **Cat-4**, and **Cat-3** indicated that steric bulk (as measured by A-values[25]) did not correlate with activity; more likely, increased ligand rigidity in the same order led to a less dense ligand/Au complex packing on the NP surface, thereby facilitating reactant access to the active sites. Finally, the presence of hydroxyl groups was critical to catalyst activity: indeed, **Cat-8** and **Cat-9** were far less active, while **Cat-10** and **Cat-11**, with densely packing dodecyl and octadecyl *N*-substituents, were completely inactive under the standard reaction conditions. Hydroxyl groups, as mentioned above, are expected, through H-bonding interactions, to facilitate the turnover-limiting proto-deauration.[13] Finally, it appears that a surface Au $4f_{7/2}$ binding energy 83.8−84.3 eV (*vide supra*) is optimal (but not sufficient: cf. **Cat-10**) for the catalyst activity in the transformation at hand.

The attachment of NHC on the surface of Au NPs not only activates the catalysts, but also installs a handle to control enantioselectivity. Leveraging the chiral NHC in the form of **Cat-1**, 16% ee is observed (entry 1 of Table S1 and Figure S44) for product **B** under the reaction conditions outlined in Figure 4 (see Table S1 for a screen of ee against other catalysts and conditions). Control experiments showed that complex **1** does not itself catalyze the transformation (entry 2 of Table S1), and that chloride abstraction from it with $AgBF_4$ leads to uncontrolled decomposition of the cationic complex, with the precipitaton of Au^0. The Au species that remain in solution are active catalysts, but afford only 2% ee (entry 3 of Table S1 and Figure S70), indicating that NHC anchoring at the NP surface is crucial for enantioselectivity in our transformation. Although 16% ee is the highest that could be attained for our system at present, this result is, to our knowledge, the first demonstration of enantioselective catalysis by NHC-ligated Au NPs, as well as by Au DEMCs.

CONCLUSIONS

In this work, we present a novel synthesis of dendrimer-encapsulated persistent carbene-ligated Au NPs in silica. The dendrimer encapsulation and silica support rendered the NPs resistant to aggregation, which allowed us to systematically modify the NHCs with little impact on NP aggregation and complex leaching. In turn, NHCs as ligands alter the oxidation state distribution of the surface Au atoms and significantly increase the activity of the Au NPs toward a model complex transformation that is typically challenging for Au NPs-allene-carboxylic acid lactonization. Note that prior to this report, NHC-Au NP catalysis was limited to hydrogenation or CO_2 electroreduction chemistry. Moreover, beyond enhanced activity and stability, ligand-derived enantioselectivity has been demonstrated in this system. The truly modular synthesis of NHC-ligated Au NPs in the presence of dendrimers, the vast array of available NHCs with excellent performance as ancillary ligands in Au catalysis, and the superb recyclability of silica-loaded NPs combine to make for a powerful new heterogeneous catalyst system that can address challenges in both heterogeneous and homogeneous Au catalysis.

ASSOCIATED CONTENT

Supporting Information

The Supporting Information is available free of charge on the ACS Publications website at DOI: 10.1021/jacs.8b01017.

General synthetic protocol, characterization method, and spectroscopy data (PDF)

AUTHOR INFORMATION

Corresponding Authors

*fdtoste@berkeley.edu
*somorjai@berkeley.edu

ORCID

Rong Ye: 0000-0002-4171-5964
Aleksandr V. Zhukhovitskiy: 0000-0002-3873-4179
F. Dean Toste: 0000-0001-8018-2198
Gabor A. Somorjai: 0000-0002-8478-2761

Present Address

[¶]Department of Chemistry and Chemical Biology, Cornell University, Ithaca, NY 14583, USA

Author Contributions

[#]R.Y. and A.V.Z. contributed equally.

Notes

The authors declare no competing financial interest.

ACKNOWLEDGMENTS

We acknowledge support from the Director, Office of Science, Office of Basic Energy Sciences, Division of Chemical Sciences, Geological and Biosciences of the US DOE under contract DEAC02-05CH11231. Resources of the Advanced Light Source, a DOE Office of Science User Facility, and work at

DOI: 10.1021/jacs.8b01017
J. Am. Chem. Soc. 2018, 140, 4144−4149

the Molecular Foundry (Proposal 4689) was supported by the same contract. We acknowledge Dr. Dan Graham and the NIH Grant EB-002027 to NESAC/BIO for the ToF-SIMS experiments. We thank Prof. A. Paul Alivisatos for the use of TEM. R.Y. and B.B.W. thank the Student Mentoring and Research Teams (SMART) program at UC Berkeley for financial support in Summer 2017. A.V.Z. is a Merck Fellow of the Life Sciences Research Foundation.

REFERENCES

(1) (a) Ye, R.; Zhukhovitskiy, A. V.; Deraedt, C. V.; Toste, F. D.; Somorjai, G. A. *Acc. Chem. Res.* **2017**, *50*, 1894−1901. (b) Ye, R.; Hurlburt, T. J.; Sabyrov, K.; Alayoglu, S.; Somorjai, G. A. *Proc. Natl. Acad. Sci. U. S. A.* **2016**, *113*, 5159−5166. (c) Witham, C. A.; Huang, W.; Tsung, C.-K.; Kuhn, J. N.; Somorjai, G. A.; Toste, F. D. *Nat. Chem.* **2010**, *2*, 36−41. (d) Gross, E.; Liu, J. H.-C.; Toste, F. D.; Somorjai, G. A. *Nat. Chem.* **2012**, *4*, 947−952. (e) Gross, E.; Shu, X.-Z.; Alayoglu, S.; Bechtel, H. A.; Martin, M. C.; Toste, F. D.; Somorjai, G. A. *J. Am. Chem. Soc.* **2014**, *136*, 3624−3629. (f) Ye, R.; Zhao, J.; Yuan, B.; Liu, W.-C.; Rodrigues De Araujo, J.; Faucher, F. F.; Chang, M.; Deraedt, C. V.; Toste, F. D.; Somorjai, G. A. *Nano Lett.* **2017**, *17*, 584−589. (g) Ye, R.; Yuan, B.; Zhao, J.; Ralston, W. T.; Wu, C.-Y.; Unel Barin, E.; Toste, F. D.; Somorjai, G. A. *J. Am. Chem. Soc.* **2016**, *138*, 8533−8537. (h) Deraedt, C.; Ye, R.; Ralston, W. T.; Toste, F. D.; Somorjai, G. A. *J. Am. Chem. Soc.* **2017**, *139*, 18084−18092. (i) Ye, R.; Liu, W.-C.; Han, H.-L.; Somorjai, G. A. *ChemCatChem* **2018**, DOI: 10.1002/cctc.201701546.

(2) Bourissou, D.; Guerret, O.; Gabbaï, F. P.; Bertrand, G. *Chem. Rev.* **2000**, *100*, 39−92.

(3) (a) Hopkinson, M. N.; Richter, C.; Schedler, M.; Glorius, F. *Nature* **2014**, *510*, 485. (b) Arduengo, A. J.; Harlow, R. L.; Kline, M. *J. Am. Chem. Soc.* **1991**, *113*, 361−363.

(4) Jacobsen, H.; Correa, A.; Poater, A.; Costabile, C.; Cavallo, L. *Coord. Chem. Rev.* **2009**, *253*, 687−703.

(5) Zhukhovitskiy, A. V.; MacLeod, M. J.; Johnson, J. A. *Chem. Rev.* **2015**, *115*, 11503−11532.

(6) (a) Crudden, C. M.; Horton, J. H.; Narouz, M. R.; Li, Z.; Smith, C. A.; Munro, K.; Baddeley, C. J.; Larrea, C. R.; Drevniok, B.; Thanabalasingam, B.; McLean, A. B.; Zenkina, O. V.; Ebralidze, I. I.; She, Z.; Kraatz, H.-B.; Mosey, N. J.; Saunders, L. N.; Yagi, A. *Nat. Commun.* **2016**, *7*, 12654. (b) Crudden, C. M.; Horton, J. H.; Ebralidze, I. I.; Zenkina, O. V.; McLean, A. B.; Drevniok, B.; She, Z.; Kraatz, H.-B.; Mosey, N. J.; Seki, T.; Keske, E. C.; Leake, J. D.; Rousina-Webb, A.; Wu, G. *Nat. Chem.* **2014**, *6*, 409−414. (c) Ling, X.; Schaeffer, N.; Roland, S.; Pileni, M.-P. *Langmuir* **2015**, *31*, 12873−12882. (d) Roland, S.; Ling, X.; Pileni, M.-P. *Langmuir* **2016**, *32*, 7683−7696.

(7) Hahn, F. E.; Jahnke, M. C. *Angew. Chem., Int. Ed.* **2008**, *47*, 3122−3172.

(8) (a) Ott, L. S.; Campbell, S.; Seddon, K. R.; Finke, R. G. *Inorg. Chem.* **2007**, *46*, 10335−10344. (b) Ranganath, K. V. S.; Kloesges, J.; Schäfer, A. H.; Glorius, F. *Angew. Chem., Int. Ed.* **2010**, *49*, 7786−7789. (c) Ranganath, K. V. S.; Schäfer, A. H.; Glorius, F. *ChemCatChem* **2011**, *3*, 1889−1891. (d) Richter, C.; Schaepe, K.; Glorius, F.; Ravoo, B. J. *Chem. Commun.* **2014**, *50*, 3204−3207. (e) Ernst, J. B.; Muratsugu, S.; Wang, F.; Tada, M.; Glorius, F. *J. Am. Chem. Soc.* **2016**, *138*, 10718−10721. (f) Ernst, J. B.; Schwermann, C.; Yokota, G.-i.; Tada, M.; Muratsugu, S.; Doltsinis, N. L.; Glorius, F. *J. Am. Chem. Soc.* **2017**, *139*, 9144−9147. (g) Lara, P.; Rivada-Wheelaghan, O.; Conejero, S.; Poteau, R.; Philippot, K.; Chaudret, B. *Angew. Chem., Int. Ed.* **2011**, *50*, 12080−12084. (h) Gonzalez-Galvez, D.; Lara, P.; Rivada-Wheelaghan, O.; Conejero, S.; Chaudret, B.; Philippot, K.; van Leeuwen, P. W. N. M. *Catal. Sci. Technol.* **2013**, *3*, 99−105. (i) Baquero, E. A.; Tricard, S.; Flores, J. C.; de Jesús, E.; Chaudret, B. *Angew. Chem., Int. Ed.* **2014**, *53*, 13220−13224. (j) Lara, P.; Suárez, A.; Collière, V.; Philippot, K.; Chaudret, B. *ChemCatChem* **2014**, *6*, 87−90. (k) Crespo, J.; Guari, Y.; Ibarra, A.; Larionova, J.; Lasanta, T.; Laurencin, D.; Lopez-de-Luzuriaga, J. M.; Monge, M.; Olmos, M. E.; Richeter, S. *Dalton Trans.* **2014**, *43*, 15713−15718. (l) Cao, Z.; Kim, D.; Hong, D.; Yu, Y.; Xu, J.; Lin, S.; Wen, X.; Nichols, E. M.; Jeong, K.; Reimer, J. A.; Yang, P.; Chang, C. J. *J. Am. Chem. Soc.* **2016**, *138*, 8120−8125.

(9) Toste, F. D.; Michelet, V. *Gold catalysis: an homogeneous approach*; World Scientific: London, 2014.

(10) (a) Vignolle, J.; Tilley, T. D. *Chem. Commun.* **2009**, 7230−7232. (b) Hurst, E. C.; Wilson, K.; Fairlamb, I. J. S.; Chechik, V. *New J. Chem.* **2009**, *33*, 1837−1840. (c) Johnson, J. A.; Makis, J. J.; Marvin, K. A.; Rodenbusch, S. E.; Stevenson, K. J. *J. Phys. Chem. C* **2013**, *117*, 22644−22651. (d) Zhukhovitskiy, A. V.; Mavros, M. G.; Van Voorhis, T.; Johnson, J. A. *J. Am. Chem. Soc.* **2013**, *135*, 7418−7421. (e) MacLeod, M. J.; Johnson, J. A. *J. Am. Chem. Soc.* **2015**, *137*, 7974−7977. (f) Man, R. W. Y.; Li, C. H.; MacLean, M. W. A.; Zenkina, O. V.; Zamora, M. T.; Saunders, L. N.; Rousina-Webb, A.; Nambo, M.; Crudden, C. M. *J. Am. Chem. Soc.* **2018**, *140*, 1576−1579. (g) Ling, X.; Roland, S.; Pileni, M.-P. *Chem. Mater.* **2015**, *27*, 414−423. (h) Wang, G.; Rühling, A.; Amirjalayer, S.; Knor, M.; Ernst, J. B.; Richter, C.; Gao, H.-J.; Timmer, A.; Gao, H.-Y.; Doltsinis, N. L.; Glorius, F.; Fuchs, H. *Nat. Chem.* **2017**, *9*, 152. (i) Ferry, A.; Schaepe, K.; Tegeder, P.; Richter, C.; Chepiga, K. M.; Ravoo, B. J.; Glorius, F. *ACS Catal.* **2015**, *5*, 5414−5420.

(11) Song, S. G.; Satheeshkumar, C.; Park, J.; Ahn, J.; Premkumar, T.; Lee, Y.; Song, C. *Macromolecules* **2014**, *47*, 6566−6571.

(12) Handa, S.; Lippincott, D. J.; Aue, D. H.; Lipshutz, B. H. *Angew. Chem., Int. Ed.* **2014**, *53*, 10658−10662.

(13) Shu, X.-Z.; Nguyen, S. C.; He, Y.; Oba, F.; Zhang, Q.; Canlas, C.; Somorjai, G. A.; Alivisatos, A. P.; Toste, F. D. *J. Am. Chem. Soc.* **2015**, *137*, 7083−7086.

(14) Kim, Y. G.; Oh, S. K.; Crooks, R. M. *Chem. Mater.* **2004**, *16*, 167−172.

(15) Jahier-Diallo, C.; Morin, M. S. T.; Queval, P.; Rouen, M.; Artur, I.; Querard, P.; Toupet, L.; Crévisy, C.; Baslé, O.; Mauduit, M. *Chem. - Eur. J.* **2015**, *21*, 993−997.

(16) Brown, T. J.; Weber, D.; Gagné, M. R.; Widenhoefer, R. A. *J. Am. Chem. Soc.* **2012**, *134*, 9134−9137.

(17) Zheng, N.; Fan, J.; Stucky, G. D. *J. Am. Chem. Soc.* **2006**, *128*, 6550−6551.

(18) Ling, X.; Schaeffer, N.; Roland, S.; Pileni, M.-P. *Langmuir* **2013**, *29*, 12647−12656.

(19) Kruse, N.; Chenakin, S. *Appl. Catal., A* **2011**, *391*, 367−376.

(20) Fernández, G. A.; Picco, A. n. S.; Ceolın, M. R.; Chopa, A. B.; Silbestri, G. F. *Organometallics* **2013**, *32*, 6315−6323.

(21) (a) Jiang, L.; Zhang, B.; Medard, G.; Seitsonen, A. P.; Haag, F.; Allegretti, F.; Reichert, J.; Kuster, B.; Barth, J. V.; Papageorgiou, A. C. *Chem. Sci.* **2017**, *8*, 8301−8308. (b) Larrea, C. R.; Baddeley, C. J.; Narouz, M. R.; Mosey, N. J.; Horton, J. H.; Crudden, C. M. *ChemPhysChem* **2017**, *18*, 3536−3539.

(22) Roth, K. E.; Blum, S. A. *Organometallics* **2010**, *29*, 1712−1716.

(23) Gaggioli, C. A.; Ciancaleoni, G.; Zuccaccia, D.; Bistoni, G.; Belpassi, L.; Tarantelli, F.; Belanzoni, P. *Organometallics* **2016**, *35*, 2275−2285.

(24) Dröge, T.; Glorius, F. *Angew. Chem., Int. Ed.* **2010**, *49*, 6940−6952.

(25) Anslyn, E. V.; Dougherty, D. A. *Modern physical organic chemistry*; University Science Books: Sausalito, 2006.

DOI: 10.1021/jacs.8b01017
J. Am. Chem. Soc. 2018, 140, 4144−4149